American Journal of Pathology, Vol. 160, No. 3, March 2002

Technical Advance

mRNA Expression Profiling of Laser Microbeam Microdissected Cells from Slender Embryonic Structures

Stefan J. Scheidl,* Sven Nilsson,* Mattias Kalén,† Mats Hellström,† Minoru Takemoto,* Joakim Håkansson,* and Per Lindahl*

From the Department of Medical Biochemistry, Göteborg University; and Angiogenetics AB,† Göteborg, Sweden*

Microarray hybridization has rapidly evolved as an important tool for genomic studies and studies of gene regulation at the transcriptome level. Expression profiles from homogenous samples such as yeast and mammalian cell cultures are currently extending our understanding of biology, whereas analyses of multicellular organisms are more difficult because of tissue complexity. The combination of laser microdissection, RNA amplification, and microarray hybridization has the potential to provide expression profiles from selected populations of cells *in vivo*. In this article, we present and evaluate an experimental procedure for global gene expression analysis of slender embryonic structures using laser microbeam microdissection and laser pressure catapulting. As a proof of principle, expression profiles from 1000 cells in the mouse embryonic (E9.5) dorsal aorta were generated and compared with profiles for captured mesenchymal cells located one cell diameter further away from the aortic lumen. A number of genes were overexpressed in the aorta, including 11 previously known markers for blood vessels. Among the blood vessel markers were *endoglin, tie-2, PDGFB,* and *integrin-β1*, that are important regulators of blood vessel formation. This demonstrates that microarray analysis of laser microbeam micro-dissected cells is sufficiently sensitive for identifying genes with regulative functions. *(Am J Pathol 2002, 160:801–813)*

The recently published drafts of the human genome sequence roughly define the complement of mammalian genes.[1,2] Consequently, analyses of cell behavior in the context of gene expression patterns will be increasingly valuable. Global expression studies are most straightforward in systems with large and accessible populations of equivalent cells such as yeast or mammalian cell cultures. Valuable results have also been generated with heterogeneous samples such as cancer tumors and whole Drosophila embryos,[3,4] but the sample complexity sets a limit as to what kind of questions might be addressed. The expression profile of certain cells or cell types cannot be resolved, and differences between samples might reflect different cell compositions rather than different transcript abundance. Also, the sensitivity of cell-specific transcripts is reduced as these mRNA are diluted with transcripts from other cell types. Methods to isolate homogenous samples *in vivo* must be adopted and refined to fully exploit the potential of expression profiles in mammalian studies.

In this article we present a procedure for microarray hybridization of RNA extracted from cells isolated with laser microbeam microdissection (LMM) and laser pressure catapulting (LPC).[5] This procedure offers several important advantages compared to previously used microdissection methods:[6–8] the sample is not in contact with any part of the equipment or the collector device during the isolation process thus dramatically reducing the risk of contamination. LMM also allows cells of any shape and size (down to pieces of chromosomes) to be cut out and catapulted. Laser microdissection offers precise control as the cells are picked individually from histological sections. No cell-specific markers are needed for the cell isolation, even populations that are recognized by morphology alone can be isolated purely. Contrary to fluorescence-activated cell sorting or magnetic bead sorting, the tissues are not exposed to collagenase digestion before cell isolation, but are fixed or frozen in their native environment conserving the RNA

Supported by the Association of International Cancer Research, The Swedish Cancer Foundation, the Inga-Britt and Arne Lundbergs Foundation, the Åke Wibergs Foundation, the Magnus Bergvalls Foundation, the Svenska Sällskapet för Medicinsk Forskning, and Göteborg University.

Accepted for publication November 14, 2001.

Address reprint requests to Per Lindahl, Department of Medical Biochemistry, Box 440, SE-405 30 Göteborg, Sweden. E-mail: per.lindahl@medkem.gu.se.

profile in a true *in vivo* state. We are primarily interested in cell fate decisions and differentiation that typically occurs in clusters of cells located in slender embryonic structures.[9] As these structures are not preserved without fixation the procedure was optimized for fixed material, which in turn makes it applicable to most cell populations. As a proof of principle, expression profiles from cells in the mouse embryonic dorsal aorta at the onset of vascular smooth muscle cell (VSMC) induction was compared to the expression profile from mesenchymal cells located one cell diameter further away from the aorta lumen. Genes encoding endothelial markers, smooth muscle cell markers, and basement membrane proteins, were consistently overexpressed in the aorta cells, confirming the accuracy of the profiles. No such markers were overexpressed in the mesenchymal cells.

Materials and Methods

Mice

C57BL/6 mice were housed at the Department of Experimental Biomedicine at Göteborg University according to Swedish animal research regulations. All experiments have been approved by the Swedish Research Animal Ethical Committee (Drnr: 213-2000). The morning of vaginal plug detection was counted as E0.5.

Fixation

The following fixatives were tested: zinc-fix (5 g $ZnCl_2$, 6 g $ZnAc_2 \times 2H_2O$, 0.1 g $CaAc_2$, in 1 L of 0.1 mol/L Tris, pH 7.4), methanol, 70% ethanol, acetone, 4% paraformaldehyde, Formoys (60 ml EtOH, 10 ml HAc, 30 ml of 40% formaldehyde), Carnoys (50 ml EtOH, 25 ml HAc), and methacarn (60 ml EtOH, 30 ml chloroform, 10 ml HAc). Animals were dissected in ice-cold phosphate-buffered saline. Tissues were immersed in respective fixative and left overnight at 4°C.

RNA Recovery and Quality Measurements

Total RNA was extracted from P14 mouse kidneys and hearts with the Qiagen RNeasy mini kit (VWR International AB, Stockholm, Sweden). RNA content was quantified with UV-spectrophotometric analysis (A260), and recovery rates are presented as percentage of RNA content in directly homogenized tissue. RNA integrity was analyzed with electrophoresis using the NorthernMax kit (Ambion Ltd, Cambridgeshire, UK). Five μg of total RNA was loaded on 1% agarose gels. The RNA quality was evaluated by incorporation of ^{32}P-labeled CTP in the first and second strand cDNA-synthesis reaction. cDNA was generated with the replacement method according to standard protocols using a polydT primer. ^{32}P-labeled CTP was added to a final concentration of 1 μCi/μl of 10 mmol/L dNTP mix. The ^{32}P-labeled cDNA was size-fractionated on a 0.8% agarose gel, transferred to nylon filter, and analyzed with a phosphoimager according to standard procedures.

Small amounts (<1 μg) of total RNA were extracted with the Micro RNA Isolation Kit (Zymo Research, Orange, CA). RNA quantities were measured with RiboGreen RNA Quantitation Kit (Molecular Probes Europe BV, Leiden, The Netherlands) in a fluorometer (TD-360; Turner Designs Inc, Sunnyvale, CA). All procedures were performed according to the manufacturers' instructions.

LMM and LPC

E9.5 mouse embryos (C57BL/6) were zinc-fixed (4°C) overnight, and then incubated 4 hours in zinc-fix with 30% sucrose. Embryos were mounted in Tissue-Tek OCT compound (Sakura Finetek, Torrence, CA) and stored at -80°C until sectioning. Frozen sections (10 μm) were mounted on plus-charged slides (SuperFrost plus; Menzel-Gläser, Braunschweig, Germany), and left to dry for 30 minutes in room temperature before storage at -80°C in boxes with silica gel. Every sixth section was mounted on a reference glass that was stained for α-smooth muscle actin (α-SMA). For laser capturing, the slides were put into zinc-fix on ice for 5 minutes to dissolve the OCT that otherwise interferes with LMM. Next, the slides were dehydrated for 30 seconds in 70%, 95%, and 99.5% ice-cold ethanol, respectively, incubated 1 minute in xylene, and dried at room temperature. Five sections were mounted on each slide and were captured in one session using the PALM Robot-MicroBeam system (P.A.L.M. Mikrolaser Technology AG, Bernried, Germany). The LPC-collected cells ($\sim$200) were solved in 40 μl of lysis buffer (Micro RNA isolation kit; Zymo) and stored at -80°C. The process was repeated until 1000 cells were collected.

RNA Extraction and T7 RNA Amplification

LMM-isolated cells in lysis buffer were thawed and centrifuged briefly before the RNA was extracted using the Micro RNA isolation kit (Zymo) according to the manufacturer's protocol. T7 RNA (aRNA) amplification was performed in three cycles mainly according to the protocol given in Wang and colleagues[10] but with the following modifications: 0.5 μl (5 μg/μl) of linear acrylamide (Ambion Ltd.) was added in the first step of oligo-dT(15)-T7 primer annealing. After second-strand synthesis, double-stranded cDNA was phenol-chloroform-isoamylalcohol extracted once and washed three times with RNase-free water (Ambion Ltd.) on Microcon 100 columns (Millipore AB, Sundbyberg, Sweden). The final volume was adjusted to 16 μl. After *in vitro* transcription with the T7 Megascript Kit (Ambion Ltd.) for 4 hours at 37°C, the reaction mixture was mixed with 460 μl of lysis buffer (GeneElute kit; Sigma-Aldrich Chemie GmbH, Munich, Germany) and the aRNA was purified according to the RNA isolation protocol provided by the manufacturer. aRNA was eluted from the column with 50 μl of water and vacuum-dried in the presence of 60 U of RNasin (Promega UK, Southampton, UK) to a volume of 5 μl. Subsequent rounds of amplification were performed as described elsewhere.[10] However, cDNA purification, *in vitro* transcription, and aRNA purification were performed as

for the first round. A detailed protocol can be downloaded from *http://cbz.medkem.gu.se/lindahl/protocols*.

Target Labeling and Microarray Hybridization

Five μg of aRNA or 100 μg of total RNA was primed with 5 μg of random hexamer (Promega UK) or 2 μg of oligo-dT primer, respectively, and labeled in a reverse transcription reaction with Cy3-dUTP or Cy5-dUTP (Amersham Pharmacia Biotech AB, Uppsala, Sweden) in a volume of 30 μl, according to standard protocols (*http://cmgm.stanford.edu/pbrown*). The differently labeled targets were combined, mixed with 1 μl of 10 μg/μl yeast tRNA, 1 μl of 10 μg/μl polyA RNA, vacuum-dried, and resuspended in 20 μl of DIGeasy hybridization buffer (Roche Diagnostics GmbH, Mannheim, Germany). The hybridization mix was placed at 100°C for 2 minutes and then at 37°C for 30 minutes before being added to the chip. Before hybridization, the glasses were rehydrated by placing them array-side down for 15 minutes over 1× standard saline citrate (SSC), fast-dried by placing them array-side up for 10 seconds on a 100°C heat block, and then baked at 80°C for 4 hours and UV cross-linked (300 mJ).

Hybridization was performed in a 40°C water bath for 12 to 18 hours under lifter coverslip (Histolab, Göteborg, Sweden) in ArrayIT hybridization cassettes (TeleChem International Inc, Sunnyvale, CA). After hybridization, the slides were washed in 2× SSC, 0.1% sodium dodecyl sulfate for 5 minutes at room temperature, 1× SSC for 5 minutes, and finally in 0.1× SSC for 5 minutes.

Array Scanning and Data Presentation

The slides were scanned (ScanArray 3000; Packard Bioscience, Meriden, CT) at laser intensity and photomultiplier tube voltage settings giving the best dynamic range for each chip in respective channel. Image segmentation and spot quantification was performed with the ImaGene software (Biodiscovery, Marina Del Rey, CA). After median local background subtraction, the $\log_2$-transformed ratios ($Cy3_{intensity}/Cy5_{intensity}$) were plotted *versus* the mean $\log_2$ intensities $0.5*(\log_2 Cy3_{intensity} + \log_2 Cy5_{intensity})$. The ratios were normalized for signal intensity variation in a non-linear intensity-dependent way using the loess function in the S-Plus software (MathSoft Inc, Surrey, UK) as described elsewhere (Dudoit S, Yang YH, Callow MJ, Speed TP, technical report no. 578, August 2000, Department of Biochemistry, Stanford University School of Medicine). A ratio *versus* intensity plot amounts to a 45° rotation of a $\log_2 Cy3_{intensity}$ *versus* $\log_2 Cy5_{intensity}$ plot, followed by scaling of the coordinates. This representation allows for intensity-dependent nonlinear normalization, but it also directly visualizes the actual expression ratios throughout the entire 16-bit range of the scanned microarray images.

Statistic Analysis

Mean $\log_2$-transformed ratios were calculated from repeated independent experiments. The genes were individually evaluated for overexpression by *t*-tests, which is applicable because the log-transformed ratios are approximately normally distributed.

Evaluation of T7 Amplification

Expression profiles were generated from nonamplified and amplified samples in the following way: the amplified heart and kidney RNA was compared in four hybridization experiments using the independently amplified samples (hybridizations A_1 to A_4). Similarly, the nonamplified heart and kidney total RNA was compared in four independent hybridizations (hybridizations T_1 to T_4). Mean $\log_2$-transformed expression ratios were calculated for both categories (see Figure 3, a, e and f).

For evaluation of the amplification effect on the relative abundance of transcripts within a sample (preservation of profiles), $\log_2$-transformed signal intensities of the heart channels from the nonamplified hybridizations (T_{1H} to T_{4H}) were compared to the heart signals from the amplified hybridizations (A_{1H} to A_{4H}) (see Figure 3b).

For evaluation of the amplification effect on expression ratios between two samples (preservation of ratios), a ratio versus ratio plot was generated and the correlation coefficent was calculated from the mean $\log_2$-transformed expression ratios $T_{1\text{-}4}$ and $A_{1\text{-}4}$ (Figure 3g).

To assess intensity-dependent correlation of the ratios, all individual arrays were compared, and ratio *versus* ratio plots for each pair were generated. Six pairs described reproducibility of nonamplified ratios (T to T comparisons). Another six pairs described reproducibility of amplified ratios (A to A comparisons). Finally, 16 plots described the correlation between nonamplified and amplified ratios (T to A comparisons). Correlations between expression ratios in the A versus A, T versus T, and T versus A pairs were calculated in an intensity-dependent way, as follows: Each ratio versus ratio plot was divided into 10 groups based on order of abundance. The 10% most abundant clones were assigned to group 1, next 10% to group 2, and so forth. The T to A plots were grouped according to order of abundance in the amplified experiments. For each group, the Pearson correlation coefficient was calculated and plotted against the $\log_2$ intensity distribution. The curves shown in Figure 3h are the loess regression lines (S-Plus software; MathSoft Inc, Surrey, UK) through the correlation coefficient plots for each category (T to T, A to A, and T to A).

Microarray Chip Design

The chips were printed with 1350 random chosen mouse sequence-verified expressed sequence tags from the I.M.A.G.E. consortium (purchased from Invitrogen Ltd, Renfrewshire, Scotland), 2400 nonsequenced clones from a normalized E16.5 head library (generously provided by Dr. Oliver Renner, Max-Planck Institute for Physiological and Clinical Research, Bad Nauheim, Germany), 5 yeast genes, and 100 selected control genes. The clones were polymerase chain reaction (PCR) amplified, purified, and resuspended in 0.2% sarkosyl, 3×

SSC and printed with the GMS 417 spotter (Affimetrix, Santa Clara, CA) onto γ-amino propyl silane-coated CMT-Gap slides (Corning International, London, UK).

Quantitative PCR

TaqMan PCR primers and labeled probes (5′ 6-FAM, 3′ 6-TAMRA) were designed for 11 genes using the Primer Express software and purchased from Applied Biosystems (Applera Sweden, Stockholm, Sweden) (sequences can be found at *http://cbz.medkem.gu.se/lindahl/taqman*). The mRNA sequences were obtained from the Celera database.

After laser microdissection and three rounds of RNA amplification, 60 ng of aorta and mesenchyme aRNA was used for first-strand cDNA synthesis. The aRNA was mixed with 4 μl of first strand buffer, 4 μl (500 μg/ml) of random hexamers (Promega UK), 2 μl of dithiothreitol, 1 μl of RNasin (Promega UK), 2 μl of ultrapure dNTPs mix (Clontech, Palo Alto, CA), and water to a final volume of 18 μl. The mixture was incubated at 65°C for 10 minutes followed by 42°C for 1 minute. Two μl of Superscript II (Invitrogen Ltd) was added and incubation at 42°C was continued for 1 hour.

The 50-cycle TaqMan PCR assay was performed in 20-μl reactions in a 384-well microtiter plate under conditions recommended by the manufacturer using 10 μl TaqMan 2× PCR Master Mix (Applera Sweden), 6 pmol of each primer, 2 pmol of probe, and 1.5 ng of cDNA (1/40 of the cDNA reaction mix) using the AB1 PRISM 9700HT realtime PCR cycler (Applied Biosystems, Foster City, CA). Each assay was repeated three times and the mean C_T-values were used for further calculations. For each amplicon a standard curve was determined using eight serial dilutions in triplicate of a mixed cDNA template obtained from heart, kidney, and brain total RNA. The relative number of target copies in each sample was interpolated from its detection threshold (C_T) value using the standard curve. Expression ratios between aorta and mesenchyme target copies were calculated and changes <20-fold were plotted against the fold changes measured on the microarray. The TaqMan measured ratios were normalized with respect to the offset of the linear fit through this plot.

Results and Discussion

Evaluation of Fixatives

The main challenge for obtaining expression profiles from laser-microdissected cells is the limited amount of RNA that can be extracted, and it is therefore important to eliminate RNA losses at any stage. It is equally important to maintain the integrity of the transcripts because reverse transcription is a prerequisite for amplification and target labeling. Several fixatives were compared to evaluate total RNA recovery, RNA quality and the RNA performance as a template for cDNA synthesis (Figure 1; a to c). Generally, compounds with good recovery rates also preserved the integrity of the RNA and generated long cDNA products. Precipitating agents such as methanol, ethanol, and acetone efficiently recovered RNA with preserved integrity, which is in line with previous reports.[11] Cross-linking agents such as 4% paraformaldehyde and Formoys were not as favorable and failed to produce but minor amounts of RNA, also in agreement with the literature.[11] Surprisingly, a zinc-based fixative performed best in our test.[12] RNA was recovered almost as efficiently as after direct homogenization, and the synthesized cDNA was of comparable length. The protection against endogenous RNases was sufficient for RNA extraction from kidneys and whole embryos, but not from pancreas, suggesting that zinc-fix has a moderate protective ability (data not shown). Contrary to the literature,[13] methacarn and Carnoys repeatedly produced low amounts of RNA in our hands (Figure 1; a to c).

The effect of paraffin and OCT-embedding on cDNA synthesis was also evaluated. Frozen samples generated large amounts of long cDNA products, and losses during OCT embedding and freezing were small if any (Figure 2).

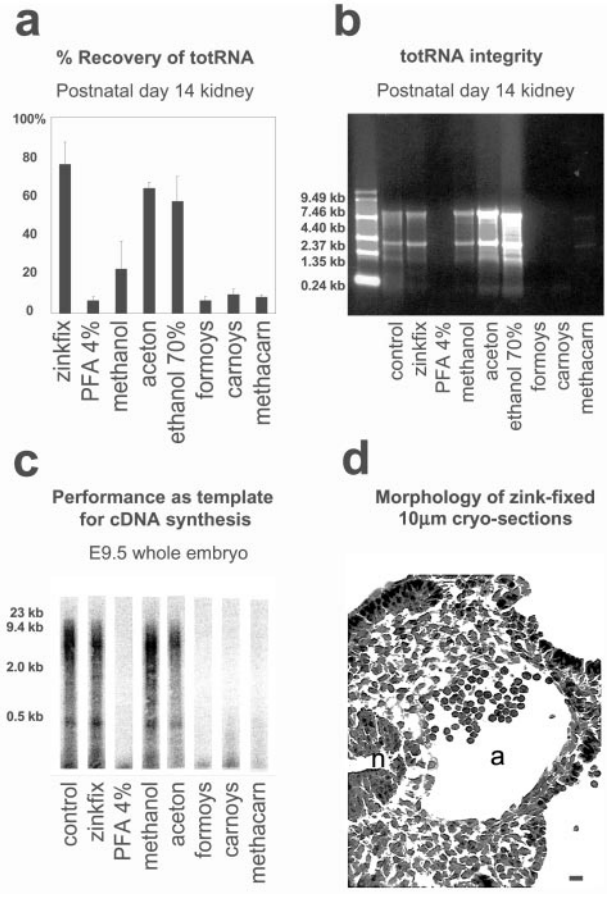

Figure 1. Several fixatives were evaluated for RNA recovery (**a**), RNA integrity (**b**), and cDNA synthesis (**c**). **a:** Kidneys from P14 mice were placed in fixative at 4°C overnight. RNA recovery is presented as percent recovery of directly homogenized tissue (error bars, 1 std). **b:** Five μg of the extracted total RNA was loaded on a denatured agarose gel for integrity evaluation. **c:** E9.5 mouse embryos were dissected and placed in fixative at 4°C overnight. Total RNA was extracted and used for synthesis of ^{32}P-labeled double-stranded cDNA. The cDNA was separated on an agarose gel, blotted to nylon filter, and visualized with a phosphoimager. **d:** Evaluation of the morphology of zinc-fixed 10-μm cryosections. Scale bar, 20 μm. n, neural tube; a, dorsal aorta.

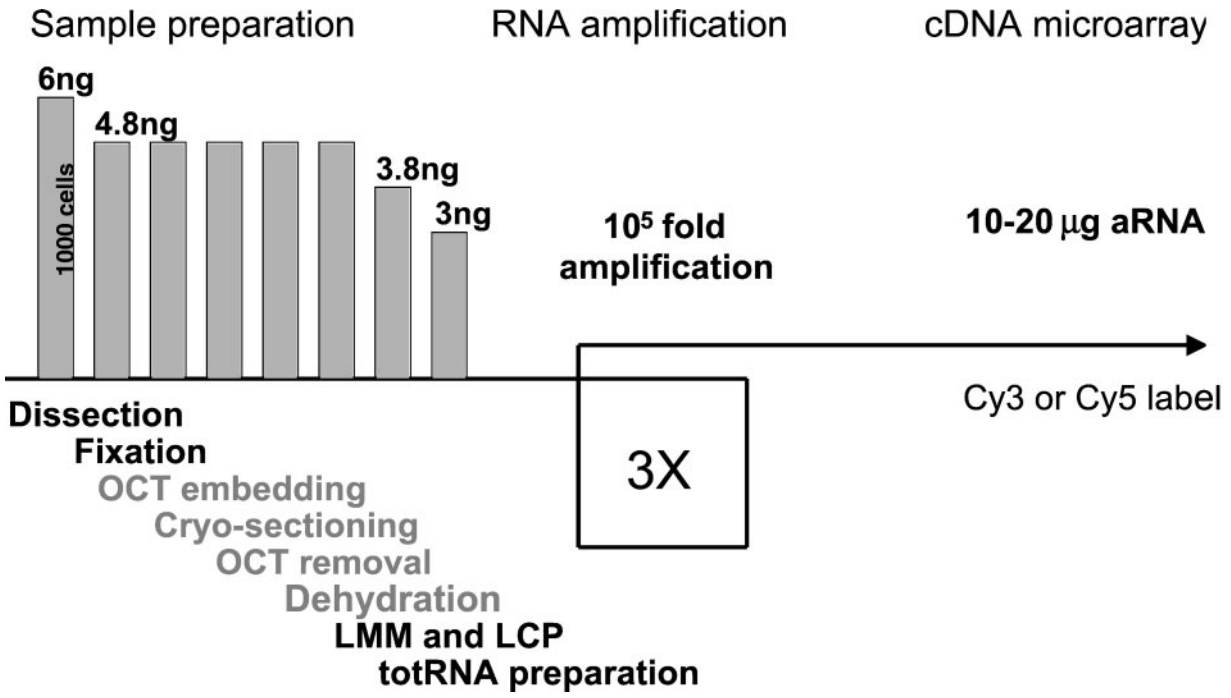

Figure 2. Schematic picture of the experimental procedure and the estimated total RNA content in the sample at various stages.

Paraffin-embedded samples also generated fair amounts of cDNA, but not comparable to frozen samples (data not shown). Although tissue morphology was superior in paraffin sections, frozen sections were of sufficient quality (Figure 1d). Most importantly, the cells preserved their relative positions despite microscopic rifts.

To summarize, zinc-fix efficiently recovers and preserves the integrity of RNA. Furthermore, zinc-fix can be performed prior to cryosectioning (contrary to precipitating agents), and was therefore chosen for all subsequent experiments.

Experimental Procedure and RNA Content

An experimental procedure for LMM and LPC isolation of cells from zinc-fixed frozen sections was worked out (Figure 2). Most of the steps are obvious necessities such as fixation, OCT embedding, cryosectioning, LMM/LPC, and RNA extraction. As LPC is most efficient with dry samples the sections were taken through a dehydration series before LMM. OCT interferes with laser cutting, and must be removed by 5 minutes of incubation in zinc-fix before dehydration. Total RNA content was measured at every step in the procedure to identify bottlenecks and to minimize losses (Figure 2). Generally, the RNA was stable when the cells were dry or frozen. RNA recovery was impaired at three steps—fixation, LMM/LPC, and RNA extraction. The evaluation of LMM/LPC and RNA extraction is discussed below. Fixation that reduces RNA recovery by ~20% has already been covered.

Laser microdissection with the PALM Robot-MicroBeam system is performed in two steps. First, the cells are outlined with a cutting laser in a process called LMM.[14] Second, the cells are vertically transferred into a collecting device held in place above (no contact) the specimen in a process called LPC. The collector is coated with sterile-filtered mineral oil (Sigma-Aldrich Chemie GmbH) to provide a sticky surface for the catapulted cells. To exclude that degradation occurs during LPC, consecutive zinc-fixed frozen sections were either deposited in mineral oil on the collector for 1 hour at room temperature, or deposited directly into homogenization buffer for 1 hour at −20°C before RNA extraction and quantification. No loss occurred in the oil (data not shown). The efficiency of LPC was initially a concern because we failed to localize the catapulted cells. A novel collector was designed to optimize cell recovery (for details see *http://cbz.medkem.gu.se/lindahl/device*). The key features of the new collector are a flat surface and free edges (no rim). This reduced the distance from specimen to collector surface from 2 mm to <100 μm. As a result, the captured cells were easy to spot and count after catapulting. Furthermore, the short distance allowed LPC with considerably less energy, which reduced the frequency of contamination caused by unintended catapulting of neighboring cells. With our specimens, ~85% of the cells could be localized on the collector.

RNA isolation and purification can be achieved through several principally different protocols. We consistently lost 40% or more of the RNA with protocols involving phenol/chloroform extraction, whereas RNA-binding matrices in spin columns typically recovered >80%. We decided to omit DNase treatment of the samples, as we otherwise had to include a phenol/chloroform extraction. We argued that: 1) DNA is a poor template for reverse transcriptase enzymes and that incorporation of T7 promotor-containing primers into DNA-encoded double-stranded cDNA is rare. 2) DNA-derived signals that

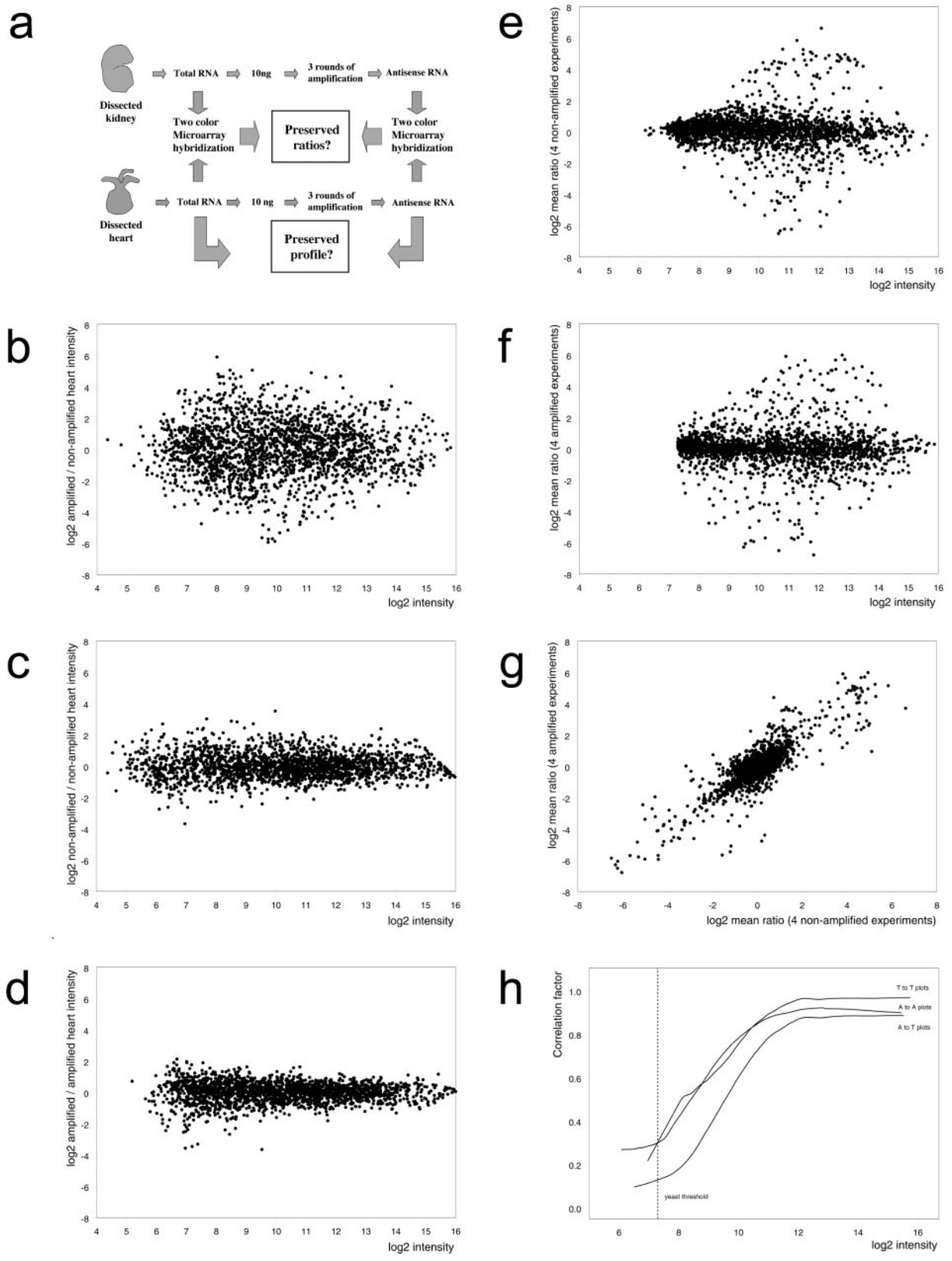

Figure 3. Evaluation of the effect of T7 amplification on microarray expression profiles. **a:** Schematic outline of the experiment. **b–d:** Evaluation of preservation of transcript abundance within samples (preservation of profiles). **e** and **f:** Expression ratios between heart and kidney for nonamplified (**e**) and amplified (**f**) RNA. **g:** Evaluation of preservation of transcript abundance difference between samples (preservation of ratios). The ratio values are taken from the graphs in (**e**) and (**f**), respectively. **h**: Evaluation of the intensity dependency of the preservation of ratios. Pearson correlation coefficients of ratio-to-ratio plots are displayed on the *y* axis, and the $\log_2$ mean intensities of the corresponding genes are displayed on the *x* axis. The graphs in **c** and **d** are generated from single experiments. The other ratio *versus* intensity graphs are generated from mean signal ratios of four repeated independent experiments.

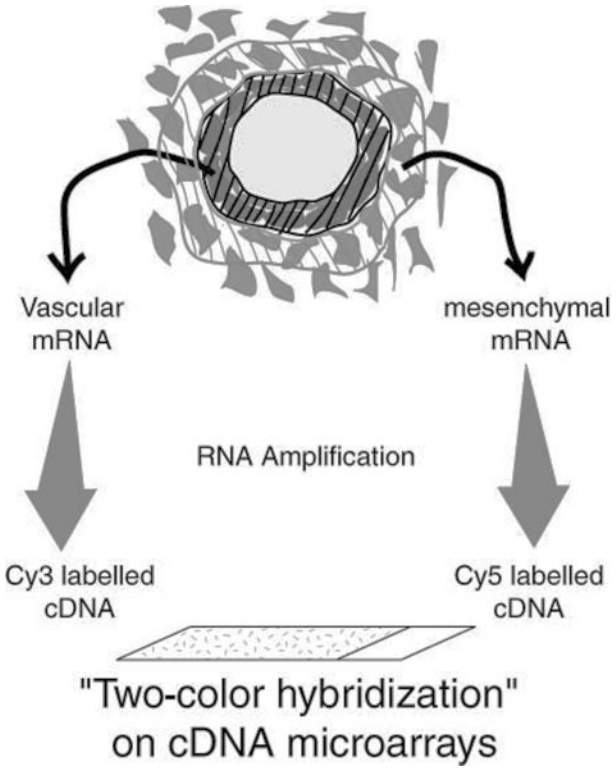

Figure 4. Schematic chart of the proof of principle experiment. Cells are isolated with LMM/LPC from: 1) the dorsal aorta, taking both endothelial and VSMCs, or from 2) local mesenchymal cells located one cell diameter further away from the vessel lumen. The samples are T7-amplified, and finally hybridized to microarrays.

bind to spots on the array will not introduce any cell-type-specific signatures, and will thus be neutral to the expression profile.

Total RNA content was quantified in mouse E9.5 dorsal aorta cells that were later captured for gene expression profiling. The numbers in Figure 2 are estimates based on measurements of RNA and DNA content in laser-microdissected cells, measurements of the average cell RNA content in whole frozen sections, and calculated losses during the experimental procedure. Our estimate, 6 pg of total RNA per cell is slightly lower than published estimates of 10 pg per cell.[15] Accordingly, 1000 laser-microdissected cells were calculated to give 2 to 3 ng of total RNA when all losses during sample preparation were considered.

Impact of T7 Amplification on Expression Profiles

The downside of all laser microdissection techniques is the labor involved because the cells are cut out individually or in small clusters. Time often sets a limit to the number of cells that can be collected. Although microarray signal detection technology and labeling methods develop rapidly, laser-microdissected material will require RNA amplification during the foreseeable future. It is critical to achieve sufficient amplification and yet maintain the expression profile. We performed a series of experiments to determine how expression profiles were affected by T7 amplification (Figure 3a). Ideally, the amplification should preserve the relative abundance of all transcripts. However, researchers are mostly interested in differences between samples, such as changes in gene expression throughout a time-course, or comparisons between a healthy state and a disease state. For these kinds of analyses, even a biased amplification is acceptable if the bias is reproducible and the differences are preserved. To address these questions, we evaluated the effect of T7 amplification on 1) the relative abundance of genes within each sample (preservation of profiles), and 2) the difference in abundance between two samples (preservation of ratios).

The expression analyses were consistently performed as two-color experiments comparing two sets of RNA, and the results are presented in ratio *versus* abundance (fluorescence intensity) plots. The ratio (*y* axis) reflects the differential expression for the given gene between the RNA sets, and the abundance (*x* axis) reflects the mean expression intensity of the gene. All values are displayed in $\log_2$ scale for convenience. Briefly, total RNA was isolated from two different sources, heart and kidney, and the gene expression was compared in two-color microarray experiments. Approximately 403 genes were more abundant in hearts, and 425 genes were more abundant in kidneys (Figure 3e, $P < 0.01$). Next, 10 ng of total RNA from the heart and kidney samples, respectively, were used for three rounds of T7 amplification. The gene expression between heart and kidney was again compared in two-color experiments using the amplified material. The approximate distribution of transcripts was preserved with 319 genes being more abundant in hearts and 370 in kidneys (Figure 3f, $P < 0.01$). The experiments were repeated four times to allow statistic analysis.

To evaluate how the amplification affected the relative abundance within samples, expression profiles from nonamplified hearts were compared to profiles from amplified hearts. Direct comparison in two-color experiments was avoided because opposite strands, sense and anti-sense RNA, are labeled in the nonamplified and T7-amplified targets, respectively. Instead, the comparisons were made with heart expression profiles obtained from different hybrizations. The expression profiles were not preserved, which indicates that there is a bias in the amplification (Figure 3b). The bias was not caused by experimental variation, because the reproducibility of T7-amplified profiles matched the reproducibility of nonamplified profiles (Figure 3, c and d). The signal intensity of microarray spots reflects gene abundance, but also transcript length and uridine content because the targets are labeled by incorporation of cyanine-conjugated dUTP. The T7-amplification protocol includes priming with random hexamers, and the transcript length is therefore systematically reduced, which could affect the profile.

We next evaluated if the amplification preserved the differences between samples: The relative abundance—the ratio of expression—of each gene was compared between heart and kidney RNA before and after amplification. The distribution of the genes that were expressed above background is shown in a plot displaying nonamplified ratios on the *x* axis and amplified ratios on the *y*

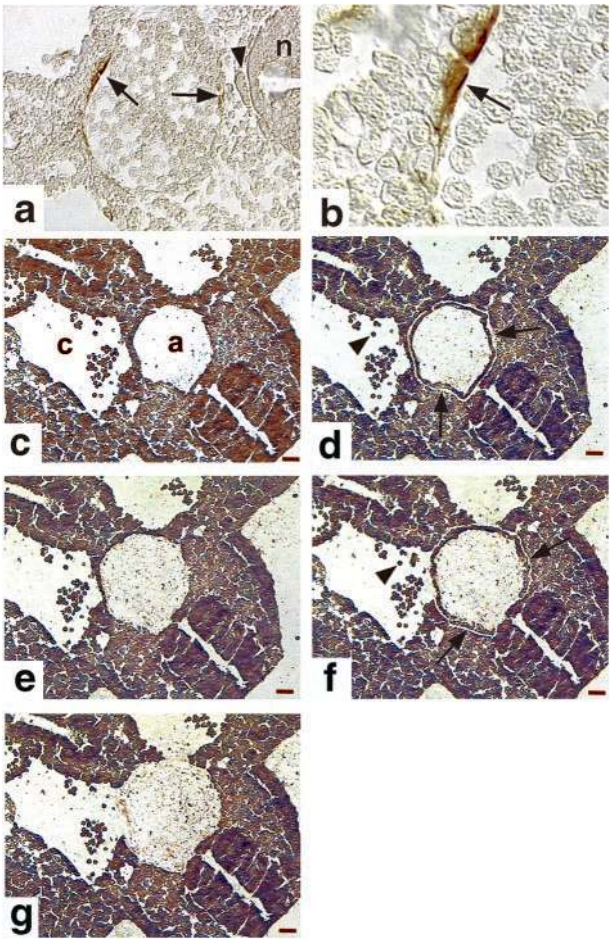

Figure 5. Endothelial and newly induced VSMCs were laser microdissected from mouse E9.5 embryonic dorsal aorta. **a** and **b:** Staining against α-SMA demonstrates smooth muscle cell differentiation in the most ventral and dorsal cells (**arrows**) but not yet in lateral cells. α-SMA staining is confined to a single layer of cells, which confirms that the cells are captured at the very onset of smooth muscle cell induction. **c–g:** Illustration of a complete laser microdissection session showing: the specimen before laser capturing (**c**), LMM of the EC/VSMC dorsal aorta cells (**d**), LPC of the dorsal aorta cells (**e**), LMM of the mesenchymal cells (**f**), and LPC of the mesenchymal cells (**g**). **Arrows** in **d, f** mark the track of the laser beam, **arrowheads** mark erythrocytes. Scale bar, 40 μm. n, neural tube; a, dorsal aorta; c, coelom; g, gut.

axis (Figure 3g). The genes are distributed along a straight line (R = 0.84 for mean ratios from four experiments), which clearly indicates that the relative abundance of a given transcript between the two samples was preserved through the amplification. The result confirms and extends previously published data.[10] A ratio *versus* ratio plot displays no information about gene abundance. To evaluate eventual effects of abundance, we divided the clones into 10 groups based on their expression intensity, and calculated the Pearson correlation coefficient (R) for each group separately (Figure 3h, A to T plots). Internal comparisons between repeated nonamplified (T to T plots) and T7-amplified experiments (A to A plots) were also included. The presented curves illustrate the impact of abundance on the preservation of expression ratios (for details, see Material and Methods). There was a striking dependence between gene abundance and degree of correlation: for high-abundance genes, the correlation was excellent with R approaching 0.90 for single experiments. For low-abundance genes, the coefficients decreased and approached 0.2 at intensities equivalent to background hybridization. Surprisingly, there was no apparent difference between repetitions of nonamplified experiments and amplified experiments. This strongly suggests that the variability in the low-abundance region derives from the microarray system and not from the amplification. The results even indicate that further rounds of amplification might be applied if need be. Another conclusion is that experiments need to be repeated many times to correctly assess low-abundance expression ratios.

LMM and Microarray Hybridization of E9.5 Aorta

The first VSMCs appear around the dorsal aorta at E9.5.[16] The cells are initially confined to the ventral and

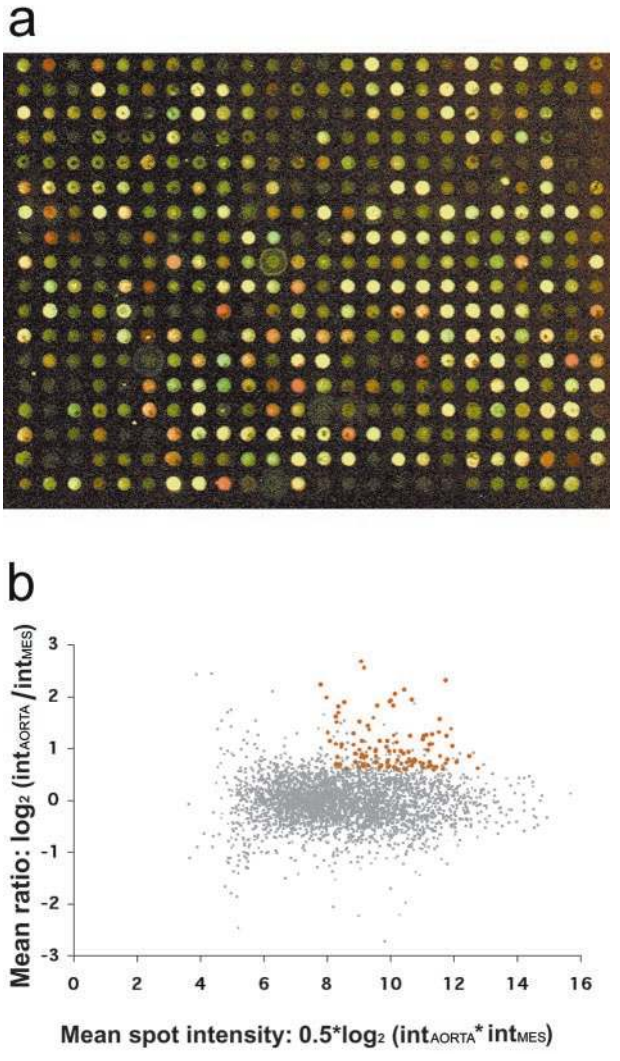

Figure 6. a: False color overlay showing part of a cDNA microarray. Spots representing aorta-overexpressed genes are red and spots representing mesenchymal genes are green. **b:** The results are presented in a scatter plot of aorta *versus* mesenchymal cells. Mean expression ratios of three independent experiments are displayed on the *y* axis, and combined mean signal intensities are displayed on the *x* axis. The diagram shows the mean values of three independent experiments. Genes that were significantly ($P < 0.05$) overexpressed (>1.5-fold) in the aorta pool are displayed in red.

Table 1. The 83 Statistically Significant (P Value < 0.05) Up-Regulated Clones with the Highest Aorta/Mesenchyme Mean Ratios (>1.5-fold) Are Listed

Fuction/Title	Gene	IMAGE _ID	GenBank _ID	UniGene _ID	-fold	*P* value
Growth factors, growth factor receptors, and related proteins						
Endometrial bleeding associated factor	Ebaf	616555	5599361	Mm.1120	1.6	0.000
Platelet-derived growth factor receptor alpha	Pdgfra				2.0	0.047
Platelet-derived growth factor beta	*Pdgfb*				*1.7*	*0.031*
Placental growth factor	Plgf				1.7	0.017
Platelet-derived growth factor alpha	Pdgfa				1.8	0.000
Insulin-like growth factor binding protein 4	Igfbp4	407845	5600267	Mm.22248	1.6	0.040
Insulin-like growth factor binding protein 2	Igfbp2	476181	5598002	Mm.141936	5.9	0.002
Endothelial-specific receptor tyrosine kinase	*Tie2*	*445565*	*5599967*	*Mm.14313*	*6.4*	*0.010*
Endoglin	*Eng*	*597174*	*4442795*	*Mm.4851*	*3.9*	*0.001*
ECM/basement membrane						
Matrix metalloproteinase 2	Mmp2	608840	5598699	Mm.29564	2.5	0.010
Procollagen, type IV, alpha 2	*Col4a2*	*571138*	*4057976*	*Mm.181021*	*3.0*	*0.000*
Procollagen, type IV, alpha 1	*Col4a1*	*599085*	*4442876*	*Mm.738*	*5.0*	*0.004*
Mediators of cell to cell and cell to matrix interactions						
Integrin beta 1	*Itgb1*	*597791*	*4442822*	*Mm.4712*	*2.4*	*0.008*
Vascular cell adhesion molecule 1	*Vcam1*	*635043*	*4058291*	*Mm.1021*	*1.5*	*0.009*
Tight junction protein 1 (ZO1)	*Tip1*	*579645*	*4060917*	*Mm.4342*	*2.1*	*0.002*
R-cadherin	Rcad				1.5	0.005
Milk fat globule-EGF factor 8 protein	Mfge8	478473	4199238	Mm.1451	2.0	0.004
Plasma membrane						
Thrombomodulin	*Thbd*	*329436*	*4199045*	*Mm.24096*	*4.7*	*0.050*
Protein with EGF-like and 2 follist.-like domains 1	Tmeff1	456713	4058601	Mm.41772	4.1	0.010
CD151 antigen	Cd151	476416	1529889	Mm.30246	2.4	0.020
Beta-2 microglobulin	B2m	596438	4442772	Mm.163	2.2	0.009
Adam12	Adam12	374232	5599832	Mm.41158	3.5	0.040
Intracellular signaling and GTPases						
Septin 2	02-sep	597545	4442806	Mm.336	1.7	0.003
Phosphoprotein enriched in astrocytes 15	Pea15	570509	4057972	Mm.544	2.2	0.002
LIM and SH3 protein 1	Lasp1	482313	4057887	Mm.21387	1.9	0.020
ADP-ribosylation-like 4	Arl4	426165	5599921	Mm.12723	1.9	0.040
ADP-ribosylation factor 4	Arf4	619051	4058243	Mm.1486	1.6	0.010
Ras homolog gene family, member C	ARHC	599288	4442887	Mm.262	1.9	0.009
Harvey rat sarcoma oncogene, subgroup R	Rras	577859	4536800	Mm.257	3.8	0.007
DNA binding/transkription factors						
TEA domain family member 1	Tead1	457517	5599982	Mm.28081	2.8	0.002
Zinc finger protein 147	Zfp147	483232	4057900	Mm.4973	2.8	0.020
SRY-box containing gene 17	Sox17	458369	5599988	Mm.5080	2.5	0.009
Csrp2/SM-lim	*Csrp2*				*2.0*	*0.002*
Early growth response 1	Egr1	608153	4059630	Mm.181959	2.0	0.002
Kruppel-like factor 7	Klf7	332349	1537938	Mm.29466	1.9	0.010
Phosphatases/kinases						
Transglutaminase 2, C polypeptide	Tgm2	635679	4058482	Mm.18843	3.8	0.020
Annexin A1	Anxa1	617853	5599493	Mm.14860	3.7	0.030
Protein tyrosine phosphatase, non-receptor type 16	Ptpn16	582081	4199621	Mm.2404	2.4	0.010
Annexin A5	Anxa5	577483	5599466	Mm.1620	2.4	0.030
Beta-galactosidase complex	Bgl	583856	4442690	Mm.2040	1.6	0.040
Apoptosis						
Caspase 6	Casp6	475851	4061226	Mm.28814	1.6	0.004
Cytoskeleton						
Highly similar to TENSIN		439464	5597960	Mm.29389	3.0	0.006
Destrin	Dsn-pending	579759	4199392	Mm.28919	2.0	0.020
Alpha smooth muscle actin	*Actvs*				*1.6*	*0.010*
Capping protein beta 1	Cappb1	408135	5599237	Mm.2945	1.5	0.000
Heparansulfate synthesis pathway Title						
Exostoses 1	Ext1				1.9	0.000
Heparan sulphate 2-O-sulfotransferase 1	Hs2st1				1.7	0.049
Lipid methabolism						
Prosaposin	Psap	406866	5600245	Mm.3363	1.7	0.000
Low-density lipoprotein receptor	Ldlr	575488	4058058	Mm.3213	1.7	0.010
Sterol-C5-desaturase	Sc5d	374370	5599096	Mm.13081	1.6	0.006
Golgi complex and ER associated proteins						
Mannoside acetylglucosaminyltransferase 1	Mgat1	579772	4060919	Mm.2672	2.4	0.010
Ribophorin II	Rpn2	425979	1436642	Mm.22130	1.7	0.010

Table 1. *Continued*

Function/Title	Gene	IMAGE _ID	GenBank _ID	UniGene _ID	-fold	*P* value
Peroxisome organization and biogenesis						
Sterol carrier protein 2, liver	Scp2	580813	4060939	Mm.1779	1.6	0.020
Peroxisomal membrane protein 3, 35 kDa	Pxmp3	534171	4536751	Mm.16453	1.5	0.050
Others						
Clusterin	Clu	409208	1401012	Mm.142594	3.8	0.020
Tre-2/USP6, BUB2, cdc16) domain family, member 1	Tbcld1	402976	5599867	Mm.27271	3.5	0.001
ESTs		317794	5599791	Mm.39047	3.1	0.004
ESTs		599146	4060460	Mm.194523	2.7	0.050
Acid sphingomyelinase-like phosphodiesterase 3a	Asml3a-pending	596904	4442786	Mm.2379	2.4	0.020
Carbonic anhydrase 3	Car3	618431	5599516	Mm.300	2.4	0.010
RIKEN cDNA 2410002J21 gene	2410002J21Rik	334438	4059149	Mm.29869	2.3	0.010
Myelin	Plp				2.2	0.041
RIKEN cDNA 2310046A13 gene	2310046A13Rik	522100	4199704	Mm.29618	2.2	0.007
Heat shock protein 20-like protein	HSP22	478560	4199241	Mm.21549	2.2	0.020
RIKEN cDNA 2210410L06 gene	2210410L06Rik	578322	1677816	Mm.22957	2.1	0.002
ESTs		582113	4199623	Mm.21463	2.1	0.040
Proteolipid protein 2	Plp2	385097	5600026	Mm.18565	2.1	0.030
FK506 binding protein 1a (12 kDa)	Fkbp1a	604923	4059572	Mm.27941	2.0	0.040
RIKEN cDNA 1500032E05 gene	1500032E05Rik	374421	5600012	Mm.7091	2.0	0.050
ESTs		473289	5598074	Mm.28044	1.9	0.030
RIKEN cDNA 2310058J06 gene	2310058J06Rik	596419	4199863	Mm.28060	1.8	0.040
ESTs		456413	4058598	Mm.76694	1.8	0.020
RIKEN cDNA 1110007H10 gene	1110007H10Rik	576642	4199567	Mm.29001	1.8	0.030
RIKEN cDNA 5330419I20 gene	5330419I20Rik	605217	5598525	Mm.142814	1.7	0.001
RIKEN cDNA 1200013D09 gene	1200013D09Rik	475947	4061230	Mm.3256	1.7	0.030
Casein kinase 1, epsilon	Csnk1e	477235	5598008	Mm.30199	1.6	0.010
Cytoplasmic polyadenylation element binding protein	Cpeb	585251	4442732	Mm.22062	1.6	0.010
RIKEN cDNA 3100004P22 gene	3100004P22Rik	476417	4061241	Mm.21819	1.5	0.040
RIKEN cDNA 1300002A08 gene	1300002A08Rik	541025	5598445	Mm.30092	1.5	0.030
RIKEN cDNA 2610027H02 gene	2610027H02Rik	583512	4199669	Mm.18249	1.5	0.002
ESTs		422784	1427022	Mm.87319	1.5	0.030
ATPase, Na+/K+ transporting, alpha 1 polypeptide	Atp1a1	482535	4198955	Mm.196547	1.5	0.006
Myxovirus (influenza virus) resistance 2	Mx2	599128	4442878	Mm.14157	1.5	0.050

The genes are sorted according to function/cellular process (www.geneontology.org). Clones that encode previously known endothelial, smooth muscle, and basement membrane markers are underlined. Twenty-eight clones from the nonsequenced set (E16.5 head cDNA library) that displayed similar statistically significant mean ratios are not listed.

dorsal aspects of the vessel, but later occur around the full circumference (see Figure 5, a and b).[17] These VSMCs probably originate from the local mesenchyme that surrounds the aorta.[18] As a proof of principle, expression profiles were generated from the endothelial cells and newly induced VSMCs of the E9.5 aorta, and compared to profiles from mesenchymal cells located one cell diameter further away from the vessel lumen (Figure 4 and Figure 5). Approximately 50 cells of each category were captured from one frozen section, and 20 sections were processed to accumulate the 1000 cells required for expression profiling. Three independent samples from aorta and mesenchyme cells, respectively, were collected, amplified, and hybridized to microarrays printed with 3800 randomly selected cDNA clones. A section of a false color overlay of such a hybridization is shown in Fig 6a.

Table 1 displays 83 statistically significant ($P < 0.05$) genes with aorta/mesenchyme mean expression ratios >1.5-fold (highlighted genes in Fig 6b). The genes fall into broad range of categories that involve most aspects of cell function. A striking number of genes belong to groups with putative regulatory functions such as growth factors, extracellular matrix components, signal transduction components, DNA binding factors, and so forth. Eleven of the genes are previously known vascular markers or markers for basement membranes,[19] which confirms the accuracy of the profiles. Among the previously known vascular markers are several genes with important regulatory functions; *Tie-2, endoglin, PDGFB,* and *integrin-β1*. Mice that lack any of these genes fail to complete various aspects of vascular development.[19]

Fifty-two statistically significant ($P < 0.05$) clones with mesenchyme to aorta expression ratios >1.5 are listed in Table 2. No genes with a previous record as vascular, smooth muscle, or basement membrane markers are found in the list.

Quantitative PCR Validation

Eleven genes were selected for validation with quantitative PCR. The analysis was performed on T7-amplified RNA from 1000 independently LMM/LPC dissected cells from E9.5 aorta and mesenchyme, respectively.

Two genes, *MMP2* and *tbc1*, did not amplify at all, probably because of insufficient optimization. The distribution of transcripts for the other genes confirmed the results from the microarray analyses (Table 3), with a Pearson correlation coefficient of 0.71 for genes with

Table 2. The 52 Statistically Significant (P Value < 0.05) Down-Regulated Clones with the Lowest Aorta/Mesenchyme Mean Ratios (>1.5-fold) Are Listed

Function/Title	Gene	IMAGE _ID	GenBank _ID	UniGene _ID	fold	*P* value
Growth factors, growth factor receptors, and related proteins						
Macrophage migration inhibitory factor	Mif	634910	4058276	Mm.2326	1.8	0.030
Protein tyrosine phosphatase, receptor type, K	Ptprk	537504	5599548	Mm.27856	1.7	0.009
Fibroblast growth factor receptor 4	Fgfr4	406823	5599876	Mm.4912	1.6	0.045
ECM/basement membrane						
Matrilin 2	Matn2	421018	1541346	Mm.3511	2.3	0.020
Plasma membrane						
CD28 antigen	Cd28	576501	4199559	Mm.1060	1.7	0.036
Intracellular signaling and GTPases						
Transducin-like enhancer of split 1	Tle1	480907	4198916	Mm.12823	1.7	0.047
DNA replication/cell cycle control						
Catalytic subunit of DNA polymerase zeta RAD54 like	Rev3l	618141	5599506	Mm.2167	1.7	0.013
Cyclin D1	Ccnd1	374778	5600017	Mm.22288	1.6	0.007
DNA binding/transkription factors						
Grainyhead					2.8	0.001
Balb/c zinc finger protein PZF (Pzf)		583631	4442680	Mm.140246	2.1	0.004
Myeloid/lymphoid or mixed-lineage leukemia	Mll	481236	4198926	Mm.2389	2.0	0.000
MutS homolog 3 (E. coli)	Msh3	596177	4442761	Mm.116254	2.0	0.041
ELAV-like 1 (Hu antigen R)	Elavl1	634761	4058259	Mm.21766	2.0	0.019
Phospholipase c neighboring	Png	596071	4442757	Mm.140	1.8	0.009
Homeo box B5	Hoxb5	421728	5599895	Mm.207	1.7	0.002
Zinc finger protein 62	Zfp62	598234	4442832	Mm.16650	1.6	0.025
Nuclear transcription factor-Y beta	Nfyb	574429	4058033	Mm.3259	1.5	0.020
Phosphatases/kinases						
Protein kinase C, delta	Pkcd	421002	5599890	Mm.2314	2.2	0.014
Cytoskeleton						
Tropomodulin 2	Tmod2	313113	4058326	Mm.44216	2.2	0.003
Alpha tubulin					1.5	0.032
Clycolysis-associated proteins						
Aldolase 3, C isoform	Aldo3	315564	1284165	Mm.7729	1.9	0.028
Enolase 3, beta muscle	Eno3	608804	4059663	Mm.29994	1.9	0.029
Lipid methabolism						
Lipoprotein lipase	Lpl	475661	4061216	Mm.1514	2.0	0.000
Proteasome-associated proteins						
26S proteasome-associated pad1 homolog	Poh1-pending	577545	5598782	Mm.27933	1.6	0.012
Proteasome subunit, alpha type 3	Psma3	534386	4199760	Mm.1007	1.5	0.012
Peroxisome organization and biogenesis						
Solute carrier family 25, member 17	Slc25a17	439854	5597964	Mm.306	1.7	0.032
Others						
RIKEN cDNA 0610025I19 gene	0610025I19Rik	317849	4058377	Mm.27395	3.2	0.004
ESTs		540165	1681385		2.5	0.006656
RIKEN cDNA 1110014J22 gene	1110014J22Rik	571623	1660309	Mm.7165	2.4	0.004
Monocyte macrophage 19	Mmrp19-pending	477887	4061333	Mm.24772	2.4	0.003
Na/taurocholate cotransporting polypeptide 1		574262	4061747	Mm.150060	2.3	0.008
ESTs		484183	5599581	Mm.19962	2.3	0.047
ESTs		401495	5599184		2.1	0.008
Glycine C-acetyltransferase	Gcat	315143	1283258	Mm.18618	2.0	0.035
ESTs		315392			2.0	0.010
RIKEN cDNA 2310012M18 gene	2310012M18Rik	493198	4057932	Mm.41438	2.0	0.019
RIKEN cDNA 2810409H07 gene	2810409H07Rik	538110	5598378	Mm.22661	2.0	0.005
Dihydrofolate reductase	Dhfr	439059	5599936	Mm.23695	1.9	0.005
FK506 binding protein 4 (59 kDa)	Fkbp4	423657	1428339	Mm.12758	1.8	0.008
ESTs		368147	5599080		1.8	0.013
RIKEN cDNA 1110033B05 gene	1110033B05Rik	407499	5599230	Mm.29145	1.8	0.007
ESTs		423973	1542767		1.8	0.015237
ESTs		476368	4061239	Mm.198722	1.8	0.001
Tousled-like kinase 2 (Arabidopsis)	Tlk2	577746	4536798	Mm.4557	1.7	0.050
RIKEN cDNA 1110003P10 gene	1110003P10Rik	475796	5597998	Mm.29051	1.6	0.048
ESTs		458629			1.62	0.033167
Nuclear autoantigenic sperm protein	Nasp	541012	5598444	Mm.7516	1.6	0.016
ESTs		315292	5599793		1.6	0.002
ESTs		424470	1428236		1.59	0.001217
ESTs		423941	1407303		1.59	0.003214
Aldo-keto reductase family 1	Akr1b1	604252	1724211	Mm.451	1.6	0.028
RIKEN cDNA 1300007E16 gene	1300007E16Rik	574092	4058026	Mm.183025	1.6	0.003
RIKEN cDNA 2810416I22 gene	2810416I22Rik	332501	1282628	Mm.12553	1.5	0.032

The genes are sorted according to function/cellular process (www.geneontology.org). No evident vascular, smooth muscle, or basement membrane markers were found. Significant clones from the nonsequenced set are not listed.

Table 3. Comparison of Fold Change Measurements Obtained with Taqman PCR and Microarray

Gene	Taqman ratio	Microarray ratio	Microarray mesenchyme signal intensity
CD151	2.5	2.4	1500
Rras	5.2	3.8	830
Klf7	3.4	1.9	540
P4ha1	0.4	1	440
Aldo1	0.6	1	3700
GAPDH	1.9	0.7	2400
Endoglin	370	3.9	130*
Tie2	240	6.3	210*
α-SMA	>1000	1.6	1600

*Signal below yeast mean signal in mesenchyme pool (threshold = 290).

<20-fold overexpression. However, the PCR-quantified ratios for *endoglin*, *tie-2*, and α-*SMA* were much higher than estimated from the array experiments, which illustrates a predicted phenomenon: the *endoglin* and *tie-2* array signal in the mesenchymal pool was not greater than the mean yeast signal. Consequently, the measured ratios reflect the difference between a significant signal in the aorta pool and background hybridization in the mesenchymal pool. Quantitative PCR, on the other hand, gives a true estimate of ratios even from rare transcripts because the background signal generated with PCR is magnitudes lower. The difference in α-*SMA* ratio might stem from use of slightly older embryos in the PCR experiment: the dorsal aortas were captured at the very onset of α-*SMA* expression, and even slight variation in age between samples might increase or decrease the number of α-*SMA*-positive cells considerably. More importantly, it has been shown that the border of α-*SMA* expression is diffuse initially with labeling of mesenchymal cells further away from the aorta lumen.[17] With time, the expression becomes confined to the vascular wall cells. Alternatively, there is cross-hybridization between actin paralogs on the array.

To summarize, this article evaluates the combination of LMM/LPC, T7 amplification, and cDNA microarray hybridization. The analysis was performed on fixed tissues, using a zinc-based fixative, that do not interfere with cDNA synthesis or T7 amplification. Stringent evaluation of the T7 amplification procedure showed a striking reproducibility. Finally, more than 80 overexpressed genes, among them 10 previously known vascular markers, were identified in a proof of principle experiment on laser-microdissected cells from the E9.5 mouse dorsal aorta. In conclusion, this article demonstrates that LMM/LPC-dissected cells are suitable for global gene expression analysis. It also shows that microarray hybridization of RNA from LMM/LPC-isolated cells is sufficiently sensitive to identify genes with key regulatory functions.

Acknowledgments

We thank Dr. Petter Mostad, Prof. Mats Rudemo, and Tatsiana Lobovkina, Department of Mathematics, Chalmers, Sweden for assistance with statistical analyses; and Anna Cederberg, Department of Medical Biochemistry, Göteborg University, Sweden, for assistance with TaqMan PCR.

References

1. Venter JC, Adams MD, Myers EW, Li PW, Mural RJ, Sutton GG, Smith HO, Yandell M, Evans CA, Holt RA, Gocayne JD, Amanatides P, Ballew RM, Huson DH, Wortman JR, Zhang Q, Kodira CD, Zheng XH, Chen L, Skupski M, Subramanian G, Thomas PD, Zhang J, Gabor Miklos GL, Nelson C, Broder S, Clark AG, Nadeau J, McKusick VA, Zinder N, Levine AJ, Roberts RJ, Simon M, Slayman C, Hunkapiller M, Bolanos R, Delcher A, Dew I, Fasulo D, Flanigan M, Florea L, Halpern A, Hannenhalli S, Kravitz S, Levy S, Mobarry C, Reinert K, Remington K, Abu-Threideh J, Beasley E, Biddick K, Bonazzi V, Brandon R, Cargill M, Chandramouliswaran I, Charlab R, Chaturvedi K, Deng Z, Di Francesco V, Dunn P, Eilbeck K, Evangelista C, Gabrielian AE, Gan W, Ge W, Gong F, Gu Z, Guan P, Heiman TJ, Higgins ME, Ji RR, Ke Z, Ketchum KA, Lai Z, Lei Y, Li Z, Li J, Liang Y, Lin X, Lu F, Merkulov GV, Milshina N, Moore HM, Naik AK, Narayan VA, Neelam B, Nusskern D, Rusch DB, Salzberg S, Shao W, Shue B, Sun J, Wang Z, Wang A, Wang X, Wang J, Wei, M, Wides R: The sequence of the human genome. Science 2001, 291:1304–1351
2. Lander ES, Linton LM, Birren B, Nusbaum C, Zody MC, Baldwin J, Devon K, Dewar K, Doyle M, FitzHugh W, Funke R, Gage D, Harris K, Heaford A, Howland J, Kann L, Lehoczky J, LeVine R, McEwan P, McKernan K, Meldrim J, Mesirov JP, Miranda C, Morris W, Naylor J, Raymond C, Rosetti M, Santos R, Sheridan A, Sougnez C, Stange-Thomann N, Stojanovic N, Subramanian A, Wyman D, Rogers J, Sulston J, Ainscough R, Beck S, Bentley D, Burton J, Clee C, Carter N, Coulson A, Deadman R, Deloukas P, Dunham A, Dunham I, Durbin R, French L, Grafham D, Gregory S, Hubbard T, Humphray S, Hunt A, Jones M, Lloyd C, McMurray A, Matthews L, Mercer S, Milne S, Mullikin JC, Mungall A, Plumb R, Ross M, Shownkeen R, Sims S, Waterston RH, Wilson RK, Hillier LW, McPherson JD, Marra MA, Mardis ER, Fulton LA, Chinwalla AT, Pepin KH, Gish WR, Chissoe SL, Wendl MC, Delehaunty KD, Miner TL, Delehaunty A, Kramer JB, Cook LL, Fulton RS, Johnson DL, Minx PJ, Clifton SW, Hawkins T, Branscomb E, Predki P, Richardson P, Wenning S, Slezak T, Doggett N, Cheng JF, Olsen A, Lucas S, Elkin C, Uberbacher E, Frazier M, Gibbs RA, Muzny DM, Scherer SE, Bouck JB, Sodergren EJ, Worley KC, Rives CM, Gorrell JH, Metzker ML, Naylor SL, Kucherlapati RS, Nelson DL, Weinstock GM, Sakaki Y, Fujiyama A, Hattori M, Yada T, Toyoda A, Itoh T, Kawagoe C, Watanabe H, Totoki Y, Taylor T, Weissenbach J, Heilig R, Saurin W, Artiguenave F, Brottier P, Bruls T, Pelletier E, Robert C, Wincker P, Smith DR, Doucette-Stamm L, Rubenfield M, Weinstock K, Lee HM, Dubois J, Rosenthal A, Platzer M, Nyakatura G, Taudien S, Rump A, Yang H, Yu J, Wang J, Huang G, Gu J, Hood L, Rowen L, Madan A, Qin S, Davis RW, Federspiel NA, Abola AP, Proctor MJ, Myers RM, Schmutz J, Dickson M, Grimwood J, Cox DR, Olson MV, Kaul R, Shimizu N, Kawasaki K, Minoshima S, Evans GA, Athanasiou M, Schultz R, Roe BA, Chen F, Pan H, Ramser J, Lehrach H, Reinhardt R, McCombie WR, de la Bastide M, Dedhia N, Blocker H, Hornischer K, Nordsiek G, Agarwala R, Aravind L, Bailey JA, Bateman A, Batzoglou S, Birney E, Bork P, Brown DG, Burge CB, Cerutti L, Chen HC, Church D, Clamp M, Copley RR, Doerks T, Eddy SR, Eichler EE, Furey TS, Galagan J, Gilbert JG, Harmon C, Hayashizaki Y, Haussler D, Hermjakob H, Hokamp K, Jang W, Johnson LS, Jones TA, Kasif S, Kaspryzk A, Kennedy S, Kent WJ, Kitts P, Koonin EV, Korf I, Kulp D, Lancet D, Lowe TM, McLysaght A, Mikkelsen T, Moran JV, Mulder N, Pollara VJ, Ponting CP, Schuler G, Schultz J, Slater G, Smit AF, Stupka E, Szustakowki J, Thierry-Mieg D, Wagner L, Wallis J, Wheeler R, Williams A, Wolf YI, Wolfe KH, Yang SP, Yeh RF, Collins F, Guyer MS, Peterson J, Felsenfeld A, Wetterstrand KA, Patrinos A, Morgan MJ: Initial sequencing and analysis of the human genome. Nature 2001, 409:860–921
3. Alizadeh AA, Eisen MB, Davis RE, Ma C, Lossos IS, Rosenwald A, Boldrick JC, Sabet H, Tran T, Yu X, Powell JI, Yang L, Marti GE, Moore T, Hudson Jr J, Lu L, Lewis DB, Tibshirani R, Sherlock G, Chan WC, Greiner TC, Weisenburger DD, Armitage JO, Warnke R, Levy R, Wilson W, Grever MR, Byrd JC, Botstein D, Brown PO, Staudt LM: Distinct types of diffuse large B-cell lymphoma identified by gene expression profiling. Nature 2000, 403:503–511

4. White KP, Rifkin SA, Hurban P, Hogness DS: Microarray analysis of Drosophila development during metamorphosis. Science 1999, 286: 2179–2184
5. Schutze K, Lahr G: Identification of expressed genes by laser-mediated manipulation of single cells. Nature Biotechnol 1998, 16:737–742
6. Luo L, Salunga RC, Guo H, Bittner A, Joy KC, Galindo JE, Xiao H, Rogers KE, Wan JS, Jackson MR, Erlander MG: Gene expression profiles of laser-captured adjacent neuronal subtypes. Nat Med 1999, 5:117–122
7. Kitahara O, Furukawa Y, Tanaka T, Kihara C, Ono K, Yanagawa R, Nita ME, Takagi T, Nakamura Y, Tsunoda T: Alterations of gene expression during colorectal carcinogenesis revealed by cDNA microarrays after laser-capture microdissection of tumor tissues and normal epithelia. Cancer Res 2001, 61:3544–3549
8. Ono K, Tanaka T, Tsunoda T, Kitahara O, Kihara C, Okamoto A, Ochiai K, Takagi T, Nakamura Y: Identification by cDNA microarray of genes involved in ovarian carcinogenesis. Cancer Res 2000, 60: 5007–5011
9. Wolpert L: Principles of Development. New York, Oxford University Press, 1998
10. Wang E, Miller LD, Ohnmacht GA, Liu ET, Marincola FM: High-fidelity mRNA amplification for gene profiling. Nature Biotechnol 2000, 18: 457–459
11. Goldsworthy SM, Stockton PS, Trempus CS, Foley JF, Maronpot RR: Effects of fixation on RNA extraction and amplification from laser capture microdissected tissue. Mol Carcinog 1999, 25:86–91
12. Johansson M, Jansson T, Powell TL: Na(+)-K(+)-ATPase is distributed to microvillous and basal membrane of the syncytiotrophoblast in human placenta. Am J Physiol 2000, 279:R287–R294
13. Shibutani M, Uneyama C, Miyazaki K, Toyoda K, Hirose M: Methacarn fixation: a novel tool for analysis of gene expressions in paraffin-embedded tissue specimens. Lab Invest 2000, 80:199–208
14. Schutze K, Posl H, Lahr G: Laser micromanipulation systems as universal tools in cellular and molecular biology and in medicine. Cell Mol Biol 1998, 44:735–746
15. Russel J: Molecular Cloning, A Laboratory Manual. New York, Cold Spring Harbor Laboratory Press, 2001
16. Takahashi Y, Imanaka T, Takano T: Spatial and temporal pattern of smooth muscle cell differentiation during development of the vascular system in the mouse embryo. Anat Embryol (Berl) 1996, 194: 515–526
17. Hungerford JE, Owens GK, Argraves WS, Little CD: Development ofthe aortic vessel wall as defined by vascular smooth muscle and extracellular matrix markers. Dev Biol 1996, 178:375–392
18. Thayer JM, Meyers K, Giachelli CM, Schwartz SM: Formation of the arterial media during vascular development. Cell Mol Biol Res 1995, 41:251–262
19. Carmeliet P: Mechanisms of angiogenesis and arteriogenesis. Nat Med 2000, 6:389–395